Inorg. Chem. **2008**, *47*, 4126−4139

Solution $[Cu(amm)]^{2+}$ is a Strongly Solvated Square Pyramid: A Full Account of the Copper K-edge XAS Spectrum Within Single-Electron Theory

Patrick Frank,*,†,‡ Maurizio Benfatto,§ Britt Hedman,‡ and Keith O. Hodgson†,‡

Department of Chemistry, Stanford University, Stanford, California 94305-5080, Stanford Synchrotron Radiation Laboratory, SLAC, Stanford University, Stanford, California 94309, and Laboratori Nazionali di Frascati-INFN, P.O. Box 13, 00044 Frascati, Italy

Received October 26, 2007

The solution structure of Cu(II) in 4 M aqueous ammonia, $[Cu(amm)]^{2+}$, was assessed using copper K-edge extended X-ray absorption fine structure (EXAFS) and Minuit XANes (MXAN) analyses. Tested structures included trigonal planar, planar and D_{2d}-tetragonal, regular and distorted square pyramids, trigonal bipyramids, and Jahn−Teller distorted octahedra. Each approach converged to the same axially elongated square pyramid, $4 \times Cu-N_{eq} = 2.00 \pm 0.02$ Å and $1 \times Cu-N_{ax}=2.16 \pm 0.02$ Å (EXAFS) or 2.20 ± 0.07 Å (MXAN), with strongly localized solvation shells. In the MXAN model, four equatorial ammonias averaged 13° below the Cu(II) *xy*-plane, which was 0.45 ± 0.1 Å above the mean N_4 plane. When the axial ligand equilibrium partial occupancies of about 0.65 ammonia and 0.35 water were included, EXAFS modeling found $Cu-L_{ax}$ distances of 2.16 and 2.31 Å, respectively, reproducing the distances found in the crystal structures of $[Cu(NH_3)_5]^{2+}$ and $[Cu(NH_3)_4(H_2O)]^{2+}$. A transverse axially localized solvent molecule was found at 2.8 Å (EXAFS) or 3.1 Å (MXAN). Six second-shell solvent molecules were also found at about 3.4 ± 0.01 (EXAFS) or 3.8 ± 0.2 Å (MXAN). The structure of Cu(II) in 4 M pH 10 aqueous NH_3 may be notationally described as $\{[Cu(NH_3)_{4.62}(H_2O)_{0.38}](solv)\}^{2+} \cdot 6solv$, solv = H_2O, NH_3. The prominent shoulder and duplexed maximum of the rising K-edge XAS of $[Cu(amm)]^{2+}$ primarily reflect the durable and well-organized solvation shells, not found around $[Cu(H_2O)_5]^{2+}$, rather than two-electron shakedown transitions. Not accounting for solvent scattering thus may confound XAS-based estimates of metal−ligand covalency. $[Cu(amm)]^{2+}$ continues the dissymmetry previously found for the solution structure of $[Cu(H_2O)_5]^{2+}$, again contradicting the rack-bonding theory of blue copper proteins.

Introduction

Copper(II) in aqueous ammonia solution invariably inhabits a mixture of ammine complexes (Figure S1 in the Supporting Information).[1,2] In room-temperature solution at high c_{NH_3}, a dynamic equilibrium exists between the aqua-tetraammine and pentaammine Cu(II) complexes. Crystal structures[3,4] of these majority equilibrium complexes, that is, $[Cu(NH_3)_4H_2O]^{2+}$ and $[Cu(NH_3)_5]^{2+}$, show highly similar equatorial tetraammine bonding, leaving any major differences axially localized. Therefore a solution-phase XAS structural determination of Cu(II) in aqueous ammonia can only be a measure of the average solution structure, with the major ambiguity residing in the axial Cu(II) ligands.

Extended X-ray absorption fine structure (EXAFS) determination is relatively insensitive to the difference in scattering potential between oxygen and nitrogen because these atoms produce photoelectron back-scattered waves of very similar phase and amplitude.[5] The Minuit X-ray absorption near edge (MXAN) spectral method uniquely describes both

* To whom correspondence should be addressed. Phone: 650-723-2479. Fax: 650-723-4817. E-mail: frank@ssrl.slac.stanford.edu.
† Department of Chemistry, Stanford University.
‡ Stanford Synchrotron Radiation Laboratory, SLAC, Stanford University.
§ Laboratori Nazionali di Frascati-INFN.

(1) Bjerrum, J.; Ballhausen, C. J.; Jørgensen, C. K. *Acta Chem. Scand.* **1954**, *8*, 1275–1289.
(2) Hathaway, B. J.; Tomlinson, A. A. G. *Coord. Chem. Rev.* **1970**, *5*, 1–43.
(3) Morosin, B. *Acta Crystallogr. B* **1969**, *25*, 19–30.
(4) Duggan, M.; Ray, N.; Hathaway, B. J.; Tomlinson, G.; Brint, P.; Pelin, K. *J. Chem. Soc., Dalton Trans.* **1980**, 1342–1348.
(5) Cramer, S. P.; Hodgson, K. O.; Stiefel, E. I.; Newton, W. E. *J. Am. Chem. Soc.* **1978**, *100*, 2748–2761.

10.1021/ic7021243 CCC: $40.75
Published on Web 04/22/2008

the bound-state electronic transitions and the continuum resonances, that is, the entire XAS spectrum, within the single self-consistent formalism of multiple scattering.[6–10] This description includes the identity of the ligand atom, the bonding environment and orbital symmetry, and both the radial and angular structural geometry. For this reason, MXAN analysis has a greater likelihood of distinguishing between oxygen and nitrogen ligation. In this event, some of the uncertainty residing in the identity of the axial ligands of Cu(II) in the experimental aqueous ammonia solution may be lifted. The physics supporting the MXAN method along with how it is distinguished from EXAFS analysis has been reviewed in an accessible way.[8,11] The influence of thermal motions (Debye−Waller effects) on XAS spectra are well-approximated over the analytical energy range by the phenomenological damping included in MXAN analyses.[12] MXAN fits generally yield coordination numbers and absorber−scatterer distances (bond lengths) equivalent in magnitude and precision to those yielded by EXAFS analysis.[13]

In this work, copper K-edge EXAFS analysis was used to find the best radial metrics model for Cu(II) in liquid aqueous ammonia solution. Following this, independent fits using the MXAN method are described. These relatively independent approaches to the XAS data provided cross-tests of the provisional models obtained for [Cu(amm)]$^{2+}$. Finally, a fully geometric structural model of Cu(II) in aqueous ammonia solution is described, and it is shown that a complete description of the XAS spectrum cannot be achieved without including distant solvent molecules. In particular, nonbonded second-shell solvent scatterers can make an important contribution to the rising-edge energy region of a K-edge XANES spectrum; a theoretical explanation of rising K-edge XAS features that is not well recognized.

Materials and Methods

A 1.00 M stock solution of $[Cu(H_2O)_5]^{2+}$ was prepared by dissolution of 1.854 g of reagent grade cupric perchlorate hexahydrate (Alfa Aesar) in 5.00 mL of deionized water in a class A volumetric flask. The experimental solution of ammoniated Cu(II), [Cu(amm)]$^{2+}$, in 4 M ammonia was prepared by dilution of 0.50 mL of the stock cupric solution and 1.35 mL of 14.8 M ammonia to 5.00 mL with deionized water to the mark within a second, class A volumetric flask. The measured pH of a so-prepared solution was 11.2. The equilibrium composition of this solution was experimentally determined using the extinction coefficients at 640 nm of $[Cu(NH_3)_4H_2O]^{2+}$ ($\epsilon_{640} = 39.6$ M^{-1} cm^{-1}) and $[Cu(NH_3)_5]^{2+}$ (ϵ_{640}=83.7 M^{-1} cm^{-1}) taken from the pioneering work of Bjerrum et al.[1] and employing the equation $A_{N_4} = [(C_t \times \epsilon_{N_5} - A_t)/[(\epsilon_{N_5}/\epsilon_{N_4}) - 1]$,[14] where A_t is the total absorbance at 640 nm, A_{N_4} is the absorbance of $[Cu(NH_3)_4H_2O]^{2+}$, C_t is the total concentration of Cu(II), and ϵ_{N_4} and ϵ_{N_5} are the extinction coefficients of the tetraammine and the pentaammine, respectively, at 640 nm. The solution speciation was also calculated using the program Medusa, written by Prof. I. Puigdomenech and available free of charge from the Royal Institute of Technology at Stockholm at http://www.kemi.kth.se/medusa/. The local version of Medusa was amended to include K_5 (0.3 M^{-5}),[2] for the production of $[Cu(NH_3)_5]^{2+}$.

For measurement of the copper K-edge XAS spectrum, the room-temperature liquid solution of 0.10 M Cu(II) in 4 M ammonia was loaded into a 2 mm Teflon spacer cell equipped with copper-free Kapton tape windows. The fill ports were sealed with a strip of the same Kapton tape. A total of two scans were measured, which were identical within error. After data collection, no discoloration was noted in the sample, and the second derivatives of the first and second scan XAS spectra were entirely superimposable.

XAS data were collected over the range of 8660.1−9868.7 eV at ambient temperature on SSRL 16-pole wiggler beam line 9-3, equipped with a Si[220] monochromator and a harmonic rejection mirror. The XAS data were measured in transmission mode as absorption spectra using in-line nitrogen-filled ionization chambers as detectors. Ring and beam line parameters included 3.0 GeV operating energy, the monochromator fully tuned at 9800 eV, and a wiggler field of 2.0 T. The raw copper K-edge data were calibrated to the first inflection point on the rising K-edge XAS of copper foil, assigned to 8980.30 eV. The copper XAS spectra were initially background-subtracted and normalized with the program Process, which is part of the EXAFSPAK suite of programs written by Prof. Graham George of the University of Saskatchewan and available free of charge at the SSRL web site, http://www.ssrl.slac.stanford.edu/~xas/xas-software.html. Prior to fitting the copper K-edge EXAFS, the normalized data were resplined within the local program PySpline.[15] This program permits a free choice of the number and positions of spline knot-points and real-time evaluation of the resultant EXAFS and its Fourier transform. For the EXAFS data reported here, the spline E_0 was 9000.00 eV, and the knot points were set at 9055.54, 9237.02, 9409.82, and 9643.61 eV, with spline polynomial orders of 2, 3, and 3, respectively. The XAS spectra so-splined produced an EXAFS Fourier transform having a nearly symmetrical first-shell peak and minimal structured intensity in the *R*-space region below 1 Å.

EXAFS spectra were fit over the range $k = 2-12.5$ Å^{-1} using FEFF 7[16,17] within the EXAFSPAK suite, as noted above. Integer values of coordination number were retained throughout, except as noted. Scattering paths with up to four legs, with 3% minimum weights, and distances out to 6 Å were considered. However, four-leg paths $N_{eq} \rightleftharpoons Cu$ and $N_{eq} \rightleftharpoons Cu \rightleftharpoons N_{eq}$, were less than half as intense as the three-leg paths $N_{eq} \xrightarrow{\longrightarrow Cu \longrightarrow} N_{eq}$ at the same distances and added nothing to the fit. Thus, for the final fits only 3-leg paths were used. Copper−ligand distances and Debye−Waller thermal parameters were independently floated variables. All the

(6) Johnson, K. E. *J. Chem. Phys.* **1966**, *45*, 3085–3095.
(7) Dill, D.; Dehmer, J. L. *J. Chem. Phys.* **1974**, *61*, 692–699.
(8) Benfatto, M.; Natoli, C. R.; Bianconi, A.; Garcia, J.; Marcelli, A.; Fanfoni, M.; Davoli, I. *Phys. Rev. B* **1986**, *34*, 5774–5781.
(9) Benfatto, M.; Della Longa, S. *J. Synchrotron Rad.* **2001**, *8*, 1087–1094.
(10) Benfatto, M.; Della Longa, S.; Natoli, C. R. *J. Synchrotron Rad.* **2003**, *10*, 51–57.
(11) Natoli, C. R.; Benfatto, M.; Della Longa, S.; Hatada, K. *J. Synchrotron Rad.* **2003**, *10*, 26–42.
(12) D'Angelo, P.; Roscioni, O. M.; Chillemi, G.; Della Longa, S.; Benfatto, M *J. Am. Chem. Soc.* **2006**, *128*, 1853–1858.
(13) Sarangi, R.; Benfatto, M.; Hayakawa, K.; Bubacco, L.; Solomon, E. I.; Hodgson, K. O.; Hedman, B. *Inorg. Chem.* **2005**, *44*, 9652–9659.
(14) Frank, P.; Gheller, S. F.; Newton, W. E.; Hodgson, K. O. *Biochem. Biophys. Res. Commun.* **1989**, *163*, 746–754.
(15) Tenderholt, A.; Hedman, B.; Hodgson, K. O. *PySpline: A Modern, Cross-Platform Program for the Processing of Raw Averaged XAS Edge and EXAFS Data*; Hedman, B., Pianetta, P., Eds.; American Institute of Physics, Stanford University: Palo Alto, CA, 2007; Vol. *882*, pp 105−107.
(16) Ankudinov, A. L.; Ravel, B.; Rehr, J. J.; Conradson, S. D. *Phys. Rev. B* **1998**, *58*, 7565–7576.
(17) Rehr, J. J.; Albers, R. C. *Rev. Mod. Phys.* **2000**, *72*, 621–654.

fitted E_0 variables for the EXAFS waves were linked within a given fit so that they remained identical while varying in concert. The scale factor, S_0, was fixed at 1.00 throughout. Stepping through the values $S_0 = 1.00-0.85$ in 0.05 steps did not significantly change the fitted Cu−N bond distances in the final fit but worsened the goodness-of-fit F-value. The fitted region of the Fourier transform was $R = 0.6-3.9$ Å, and so the total number of statistically independent data points,[18] N_I, for the fitted data was $N_I = (2 \times \delta k \times \delta R/\pi) + 2 = 24$. The total number of degrees of freedom in any EXAFS fit was $(2n + 1)$ where n is the number of individual waves and never exceeded 17. The weighted goodness-of-fit F-value minimized during the fit was

$$F = [\sum k^6(\chi_{exptl} - \chi_{calcd})^2/\sum k^6(\chi_{exptl})^2]^{1/2}$$

where the summation is over the fitted k-range, k is the photoelectron wave vector, and χ is the experimental or calculated data point. Cartesian coordinates for the various synthetic structural models of $[Cu(amm)]^{2+}$ used in FEFF 7 input files were derived using the program CS Chem 3D Pro (CambridgeSoft, Cambridge MA). For the entirely synthetic models, the initial equatorial Cu−N bond distances were set to 2.02 Å;[19] otherwise the crystal structure values were used. The reported statistical errors in the bond lengths are those calculated by the fit. The systematic errors in the bond lengths were determined by holding the best-fit Debye−Waller values constant while stepping the value of E_0. The variation in bond length with E_0 was recorded, and the systematic error is defined as plus or minus half the variation in bond length over the goodness of fit $\Delta F = 1$, where $F = \sum[(\chi_{exptl} - \chi_{fit})^2]$.[20]

MXAN is a new software application incorporating the well-established full multiple-scattering theoretical approach to K-edge X-ray absorption spectra,[8,21] with the aim of deriving both geometric and metrical information about metal-containing sites. This method has been described in detail elsewhere.[9,10] In the MXAN analyses, the inverse of the scattering path operator was computed exactly, avoiding any a priori selection of the relevant MS paths in the calculation of the X-ray absorption cross section. The muffin-tin (MT) approximation was used for the shape of the potential.[22] Hydrogen atoms were included in the calculation.

The MT radii were chosen to have the best agreement between theory and experimental data, and the values were 0.2, 0.86, 0.90, and 1.23 Å for hydrogen, nitrogen, oxygen, and copper, respectively. The real part of the exchange term was calculated as the Hedin−Lundqvist energy-dependent potential, while the inelastic losses were taken into account using a phenomenological method described in detail.[9−11,21] The optimization in parameter space was achieved by the minimization of the square residual function, R_{sq}, defined as

$$R_{sq} = n\frac{\sum_{i=1}^{m} w_i[(y_i^{theor} - y_i^{exptl})\epsilon_i^{-1}]^2}{\sum_{i=1}^{m} w_i}$$

where n is the number of independent parameters, m is the number of data points, y_i^{theor} and y_i^{exptl} are the theoretical and experimental values of absorption, respectively, ϵ_i is the individual error in the experimental data set, and w_i is a statistical weight. For w_i = constant = 1, the square residual function R_{sq} becomes the statistical χ^2 function.

In this work, we assumed w_i = constant=1 and the experimental error ϵ = constant = 1.0% of the main jump for the whole experimental data set. During the fitting procedure, hydrogen atoms rigidly followed the nitrogen (oxygen) movements. The floated variables in an MXAN fit included $N_{1,2}$, and $N_{3,4}$, that is, two sets of two equatorial bond lengths that were linked transversely, the axial bond lengths, N_{ax}, and the angles, $\Theta_{1,2}$ and $\Theta_{3,4}$, between the z-axis and the equatorial plane. For fits to octahedral models, the two axial bond lengths could be linked or floated separately. Thus, the MXAN calculations were allowed to find best-fit structures relaxed away from rigidly symmetrical geometries. The floated parameters are here illustrated for clarity Second-shell

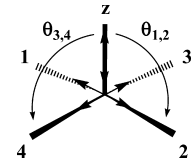

waters, when included, were also modeled as transverse pairs of molecules with linked distances and angles unless otherwise noted. The statistical errors calculated by the MIGRAD routine are quoted for brevity only for the best-fit geometry whose metric is reported in Table 5. MXAN also introduces a systematic error into the bond length of the order 1−2% that must be added to the statistical error calculated by the program.

Results

The experimental solution of 0.10 M Cu(II) in 4 M ammonia was prepared to maximize equatorial substitution of water by ammonia ligands.[23,24] Quantitative assay in terms of two components using the visible absorption band centered at 612 nm (see Materials and Methods section), indicated 32% $[Cu(NH_3)_4H_2O]^{2+}$ and 68% $[Cu(NH_3)_5]^{2+}$ in the solution used for XAS study. However, an analysis of the experimental solution in terms of known equilibrium constants (Figure S1 in the Supporting Information) indicated the slightly different composition of 30% and 63%, respectively, with about 7% of the copper also within the $[Cu(NH_3)_3(OH)]^+$ complex ion, all formulas neglecting full specification of the axial ligands. Nevertheless, the results of this work are not materially impacted by the possible presence of the minority hydroxide complex ion because XAS spectra are relatively insensitive to contributions from minority components of less than about 10% (e.g., Figure S2 in the Supporting Information), especially when such components are structurally similar to the dominant complex.

Figure 1 shows the EXAFS and Fourier transform (FT) of the EXAFS for 0.10 M Cu(II) in 4 M aqueous ammonia solution. The EXAFS exhibits the declining amplitude envelope and simple sinusoid of a single shell of low-Z scatterers. In its turn the nonphase-corrected Fourier transform spectrum is dominated by a single first shell peak at

(18) Stern, E. A. *Phys. Rev. B* **1993**, *48*, 9825–9827.
(19) Carrera, F.; Marcos, E. S.; Merkling, P. J.; Chaboy, J.; Muñoz-Paez, A. *Inorg. Chem.* **2004**, *43*, 6674–6683.
(20) IXS Error Reporting Recommendations: A Report of the Standards and Criteria Committee, 2000, http://ixs.iit.edu/IXS/subcommittee_reports/sc/err-rep.pdf.
(21) Benfatto, M.; Della Longa, S.; D'Angelo, P. *Phys. Scr.* **2005**, *T115*, 28–30.
(22) Grant, I. P.; Whitehead, M. A. *Mol. Phys.* **1976**, *32*, 1181–1185.
(23) Yamaguchi, T.; Ohtaki, H. *Bull. Chem. Soc. Jpn.* **1979**, *52*, 415–419.
(24) Prenesti, E.; Daniele, P. G.; Toso, S. *Anal. Chim. Acta* **2002**, *459*, 323–336.

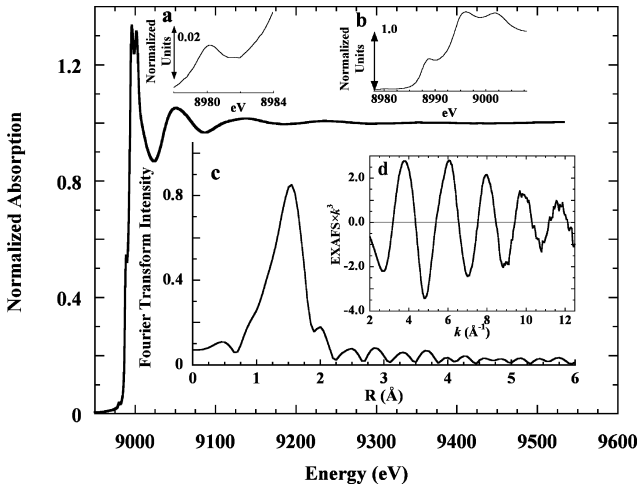

Figure 1. K-edge X-ray absorption spectrum of 0.10 M Cu(II) in 4 M aqueous ammonia solution. Inset a: Expansion of the pre-edge energy region of the spectrum. Inset b: Expansion of the rising edge region of the spectrum. Inset c: Fourier transform of the EXAFS portion of the spectrum. Inset d: the EXAFS spectrum.

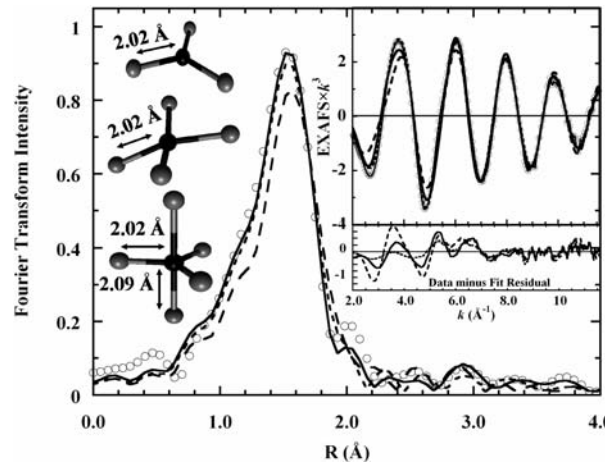

Figure 2. (○) Fourier transform of the EXAFS spectrum of 0.10 M Cu(II) in 4 M aqueous ammonia solution; (- - -) trigonal model fit to the spectrum; (- - -) tetragonal model fit to the spectrum; (—) trigonal bipyramidal fit to the spectrum. Inset top: the EXAFS spectrum and the fits to the EXAFS. The line-types have the same significance. Inset bottom: the (data minus fit) residual for each of the fits. The left margin shows cartoons and metrics of the initial models. See text for details.

1.53 Å. Four small features appearing between about 2.4 and 3.9 Å principally reflect first-shell multiple scattering or second-shell single scattering,[25] and have been observed in the Fourier transformed EXAFS spectra of room temperature aqueous or ammoniacal solutions of several transition metal ions.[25–28] The four high-R FT features exhibited ~3:1 signal-to-noise, indicated by comparison of integrated Fourier intensities over the ranges of 2.28−3.85 and 3.91−5.49 Å (Figure 1, inset c). These four features proved central to choosing among various EXAFS structural models.

EXAFS Analysis. The three-dimensional Cartesian models used to ensure a complete inventory of possible coordination environments for Cu(II) in aqueous ammonia included regular trigonal planar $[Cu(NH_3)_3]^{2+}$, square planar $[Cu(NH_3)_4]^{2+}$, trigonal bipyramidal or square pyramidal $[Cu(NH_3)_3L_2]^{2+}$, and octahedral $[Cu(NH_3)_4L_2]^{2+}$, where L = NH_3, H_2O. All models with axial ligands were tested in elongated and compressed versions.

The Fourier transforms of the EXAFS fits resulting from application of the trigonal, the square planar, or the axially elongated trigonal bipyramidal model are shown in Figure 2, along with input Feff models. Two trigonal bipyramidal fits were found that differed in axial bond length. The first included three equatorial N scatterers at 2.02 Å and two axial N,O scatterers at 2.76 Å, $F = 0.2058$. The second differentially included two axial scatterers at 2.10 Å, $F = 0.1349$. Of these, the long axial model produced a fit very similar to that of the purely trigonal model (see Figure 2).

In the Fourier transform XAS spectrum, only the tetragonal and the short axial trigonal bipyramidal models adequately fit the first-shell FT feature. However, all three models produced poor fits to the smaller feature at 2.2 Å. Multiple scattering paths within both the tetragonal and trigonal bipyramidal fits partly reproduced the four small features at $R = 2.5-4$ Å. Figure 2 inset shows that all three models successfully reproduced the phase and the shape of the EXAFS amplitude envelope. However, the EXAFS unfit residuals of the three fits (Figure 2, inset) contained obvious periodic intensities at lower k-values indicating that these models could not fully reproduce the EXAFS spectrum. Fits using an even more greatly axially compressed trigonal bipyramidal model ($4 \times Cu-N_{eq} = 2.04$ Å; $2 \times Cu-N_{ax} = 2.02$ Å, $F = 0.1369$)[29,30] produced a similar unfit residual. Therefore, all three models, trigonal $[Cu(NH_3)_3]^{2+}$, tetragonal $[Cu(NH_3)_4]^{2+}$, and trigonal bipyramidal $[Cu(NH_3)_5]^{2+}$, were rejected as viable candidates for the solution structure of $[Cu(amm)]^{2+}$.

Several square pyramidal or octahedral models were then tested, with the initial structural metrics obtained from the crystal structures of $[Cu(NH_3)_4(H_2O)]SO_4$ or $K[Cu(NH_3)_5](PF_6)_3$.[3,4] These two structures differ primarily in the identity and bond length of the axial ligand, with $Cu-L_{ax} = 2.34$ or 2.19 Å for $L_{ax} = H_2O$ or NH_3, respectively. Using these metrics as a guide, a series of models that incorporated variations in axial distances were constructed.

In the course of these fits, goodness-of-fit and Debye−Waller values were found to minimize for axial bond lengths near 2.2 or 2.8 Å. Figure 3 shows the trend in fit values using an octahedral model, while Figure S3 in the Supporting Information shows the analogous results for the square pyramidal model. In light of this result, fits to the EXAFS using the square pyramidal or octahedral models explored both short and long axial bond lengths. The fit F-values for axial bond lengths of ~2.2 and ~2.8 Å differed only slightly

(25) Kuzmin, A.; Obst, S.; Purans, J. *J. Phys.: Condens. Matter* **1997**, *9*, 10065–10078.
(26) Sakane, H.; Miyanaga, T.; Watanabe, I.; Matsubayashi, N.; Ikeda, S. *Jpn. J. Appl. Phys. 1* **1993**, *32*, 4641–4647.
(27) Lee, S.; Anderson, P. R.; Bunker, G. B.; Karanfil, C. *Environ. Sci. Technol.* **2004**, *38*, 5426–5432.
(28) Nilsson, K. B.; Eriksson, L.; Kessler, V. G.; Persson, I. *J. Mol. Liq.* **2007**, *131−132*, 113–120.
(29) Scott, M. J.; Lee, S. C.; Holm, R. H. *Inorg. Chem.* **1994**, *33*, 4651–4662.
(30) Murakami, T.; Takei, T.; Ishikawa, Y.; Kita, S. *Polyhedron* **1996**, *15*, 4391–4398.

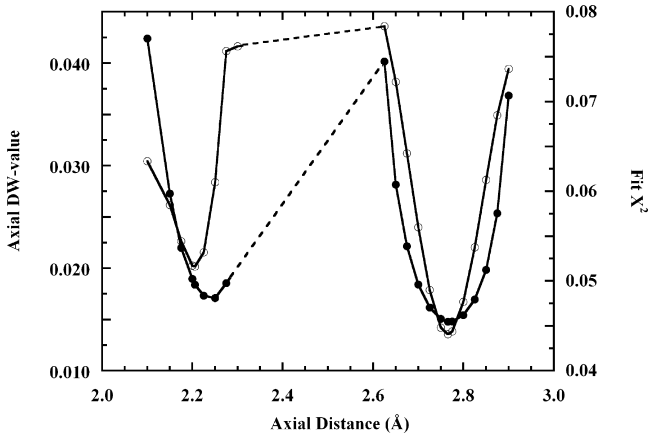

Figure 3. Double-*y* plot of (left ordinate; ●) Debye−Waller value and (right ordinate; ○) the fit χ^2 [$\sum$(fit residuals)^2/(no. points)], versus the axial bond length, in fits to the copper K-edge EXAFS spectrum of 0.1 M Cu(II) in 4 M NH_3, using a symmetric octahedral model. For axial bond lengths between 2.3 and 2.6 Å, the fits diverged. See Figure S3 in the Supporting Information for the analogous results using an elongated square pyramidal model.

for the square pyramidal model but by about 2 units for the octahedral model, in each case favoring the longer axial distance.

The best fits using the square pyramidal and octahedral models are compared in Figure S4 and Table S1 in the Supporting Information. The best fits invariably included an elongated axial distance of ~2.8 Å, with a comparatively large axial Debye−Waller value. Figure S4 shows that the square pyramidal and octahedral models produced nearly indistinguishable fits between 0.5 Å−1.8 Å, where the Fourier spectrum is dominated by the equatorial ligands. However, the octahedral model produced the better fit (F = 0.1319) and reproduced an EXAFS fit previously reported by others.[28] It is interesting to note that a ~2.8 Å axial water or ammonia is nearly beyond bonding distance.[31] These models might thus be better described as representing tetragonal complexes with strong axial solvation.

Neither the square pyramidal nor the octahedral fit adequately reproduced the small higher-R Fourier features that are associated with first-shell multiple scattering and second-shell single-scattering resonances (Figure S4 inset in the Supporting Information).[25,32,33] Given this result and the double minima shown in Figure 3, an axially dissymmetric model that included both axial distances was constructed and tested. As noted above, an axial O,N at ~2.8 Å is beyond bonding distance,[31] and so a dissymmetric model with axial scatterers at ~2.2 Å and ~2.8 Å is again better-described as a -z axially solvated square pyramidal complex. The results from the three structural models that produced the best fits at this stage are shown in Table 1. Compared with the axially elongated octahedral model (F = 0.1319), the axially dissymmetric model (F = 0.1248) slightly improved the fit to the first shell Fourier feature. The latter fit was poorer near R = 1.8 Å but significantly improved in the high-R Fourier region. Overall, the fit using the axially dissymmetric model produced a decrease in F-value of 1.4 units relative to the core axially elongated square pyramidal fit, and 0.7 units relative to the axially elongated octahedral model fit (Table 1).

However, the axially dissymmetric model included 11 degrees of freedom compared to 9 degrees of freedom for both the square pyramidal and octahedral fits. Therefore, the fit using the octahedral model was repeated allowing the two axial ligand distances to float separately, from an initial value of 2.76 Å. This fit, now also with 11 degrees of freedom, was virtually identical to its more constrained predecessor. The axial ligand bond lengths bifurcated to 2.75 and 2.77 Å, and the F-value remained unimproved at 0.1319. This result shows the favorable F-value associated with the axially dissymmetric fit is not a statistical artifact. The fits for the axially dissymmetric and the equivalently freed axially elongated octahedral models are compared in Figure 4 and the fit metrics are given in Table S2 in the Supporting Information.

As noted above, the high-R Fourier features have been interpreted to include contributions from both first-shell multiple scattering and second-shell single scattering.[25,32–35] The second shell represents an immediate solvent shell. A DFT study of gas-phase tetragonal $[Cu(NH_3)_4]^{2+}\cdot 4NH_3$ indicated a stable arrangement of four second-shell ammonia molecules at 2.8 Å.[36] Therefore the possibility of second shell contributions to $[Cu(amm)]^{2+}$ in aqueous ammonia was tested by expansion of the octahedral and axially dissymmetric models to include four second-shell solvent N,O scatterers at either 2.8 or 3.5 Å. These were distributed to bisect the four 90° first-shell equatorial N−Cu−N angles. FEFF inputs were calculated from these models, and EXAFS fits were carried out incorporating the single scattering paths from the distant solvent molecules.

Incorporation of the DFT model by addition of four distant scatterers to the axially elongated octahedral and the axially dissymmetric models markedly improved the fits to the high-R Fourier features, with the latter model distinctly superior (F = 0.1102 and 0.0971, respectively). However, a best-integer search of the EXAFS data produced an F-value minimum with six second-shell N,O scatterers, rather than four (Figure 5, inset b). With the six O,N second-shell metric, the fit produced by the axially dissymmetric model (F = 0.0965) was notably better than that of the axially elongated octahedral model (F = 0.1103) that again included two separately floated axial ligand distances. The equivalent number of fit degrees of freedom makes this comparison unambiguous. The octahedral and axially dissymmetric fits are directly compared in Figure S5; the Fourier transforms of the fits are shown in Figure S6, and the fit metrics are presented in Table S3. Figure S7 in the Supporting Informa-

(31) Harding, M. M. *Acta Crystallogr.* **1999**, *D55*, 1432–1443.
(32) Filipponi, A.; D'Angelo, P.; Pavel, N. V.; Di Cicco, A. *Chem. Phys. Lett.* **1994**, *225*, 150–155.
(33) Muñoz-Páez, A.; Pappalardo, R. R.; Sánchez Marcos, E. *J. Am. Chem. Soc.* **1995**, *117*, 11710–11720.
(34) Sakane, H.; Muñoz-Páez, A.; Diaz-Moreno, S.; Martinez, J. M.; Pappalardo, R. R.; Marcos, E. S. *J. Am. Chem. Soc.* **1998**, *120*, 10397–10401.
(35) Campbell, L.; Rehr, J. J.; Schenter, G. K.; McCarthy, M. I.; Dixon, D. *J. Synchrotron Rad.* **1999**, *6*, 310–312.
(36) Berces, A.; Nukada, T.; Margl, P.; Ziegler, T. *J. Phys. Chem. A* **1999**, *103*, 9693–9701.

Table 1. Fits for the Best Three Primitive EXAFS Models

model	CN[a]	R (Å)[b]	DW[c]	CN	R (Å)	DW	ΔE (eV)	F[d]
sq pyr	$4N_{eq}$	2.02	0.00685	$1N, O_{ax}$	2.76	0.00890	−12.46	0.1393
	$8N_{ms}$	3.96	0.00995	$4N, O_{ms}$	4.19	0.00229		
O_h(elong)	$4N_{eq}$	2.02	0.00683	$2N, O_{ax}$	2.76	0.01499	−12.14	0.1319
	$8N_{ms}$	4.78	0.01614	$4N_{ms}$	5.75	0.01210		
sq pyr_{solv}	$4N_{eq}$	2.02	0.00681	$1N, O_{ax}$	2.16	0.01896	−10.78	0.1248
	$1N, O_{ax}$	2.77	0.00959	$8N_{ms}$	4.27	0.02306		
	$4N_{ms}$	4.70	0.00257					

[a] Coordination number. [b] The errors in bond lengths are as follows: first shell, $(\pm 0.003$ Å$)_{ste}(\pm 0.01$ Å$)_{sys}$; short axial shell $(\pm 0.01$ Å$)_{ste}(\pm 0.02$ Å$)_{sys}$; long axial shell $(\pm 0.01$ Å$)_{ste}(\pm 0.04$ Å$)_{sys}$, where ste represents the statistical error, and sys represents the systematic error. [c] Debye−Waller value. [d] Goodness-of-fit F value, as percent. Subscripts: eq is equatorial; ax is axial; ms is multiple scattering.

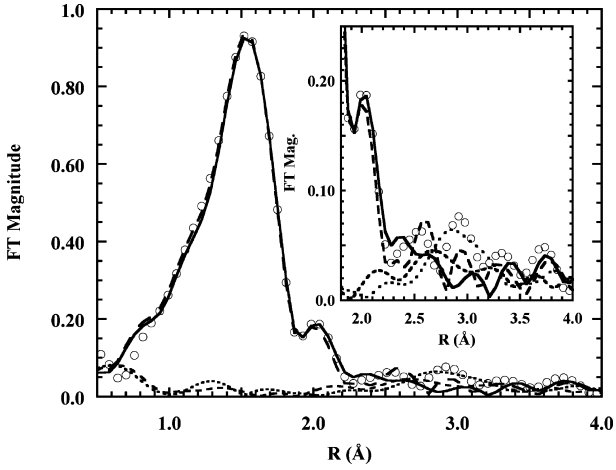

Figure 4. (○) Fourier transform K-edge EXAFS spectrum of 0.10 M Cu(II) in 4 M aqueous ammonia. (—) The fit using an octahedral model with two independently floating, but similar, axial distances. (···) The FT unfit residual. (− −) The fit using the axially dissymmetric model. (---) The FT unfit residual. The inset shows an expansion of the high-R portion of the Fourier transform, the fits, and the unfit residuals. The line-types have the same significance.

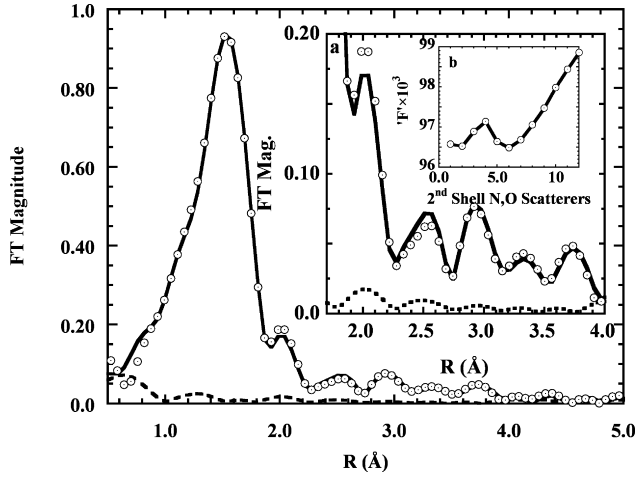

Figure 5. (○) Fourier transform of the copper K-edge EXAFS of 0.1 M Cu(II) in 4 M aqueous ammonia solution, with (—) the Fourier transform of the fit using the axially dissymmetric model plus six distant N,O scatterers and (**- - -**) the unfit Fourier residual. Inset a: Expansion of the high-R portion of the FT spectrum. The line types have the same significance. Inset b: Best-integer second-shell fit, showing the F-value minimum for six second-shell N,O scatterers. The F minimum at 2 N,O scatterers was accompanied by a cross-correlation between the 2- and 3-leg equatorial paths, which produced large Debye−Waller values. See Figure S5 and Figure S6 in the Supporting Information for a comparison of this fit with the analogous fit using the $J-T$ octahedral model.

tion shows that the fit using the axially dissymmetric model ($F = 0.0965$) is slightly better than that obtained by averaging two symmetrical octahedral models with two short or two

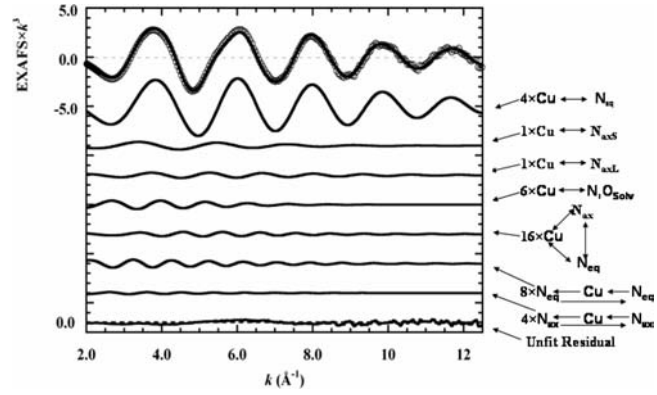

Figure 6. (○) K-edge EXAFS spectrum of 0.10 M Cu(II) in room temperature 4 M aqueous ammonia solution and (—) the final fit to the spectrum using the axially dissymmetric model plus six solvent N,O scatterers, as discussed in the text. The individual scattering paths are designated to the right. The bottom line shows the data minus fit residual and a dashed zero reference. Subscripts: eq = equatorial, ax = axial, S = short, L = long, and solv = solvent.

Table 2. Metrics of for the Final Fit to the EXAFS: Axially Dissymmetric Model plus Six Second-Shell N,O Scatterers

CN	R (Å)[b]	DW	CN	R (Å)	DW	ΔE (eV)	F-value
$4N_{eq}$[a]	2.02	0.00673	$1N_{ax}$	2.16	0.01789	−9.00	0.0965
$1N_{ax}$	2.77	0.01040	$6N, O_{solv}$	3.40	0.03026		
$16N_{ms}$	3.90	0.00952	$8N_{ms}$	4.22	0.00558		
$4N_{ms}$	4.66	0.01053					

[a] Subscripts have the meaning given in Table 1. [b] The errors in bond-lengths are as follows: first shell, $(\pm 0.001$ Å$)_{ste}(\pm 0.01$ Å$)_{sys}$; short axial shell $(\pm 0.01$ Å$)_{ste}(\pm 0.06$ Å$)_{sys}$; long axial shell $(\pm 0.01$ Å$)_{ste}(\pm 0.03$ Å$)_{sys}$, where ste represents the statistical error, and sys represents the systematic error.

long axial distances, respectively, $F_{av} = 0.1165$. This result vitiates the possibility that the dissymmetric model is fitting the EXAFS of an equilibrium mixture of two octahedral complex ions, differing only in the $Cu-L_{ax}$ distance.

The Fourier transform of the EXAFS and the final fit using the axially dissymmetric model including six second-shell N,O scatterers is shown in Figure 5. The final fit to the EXAFS spectrum including all the individual paths and the unfit residual is shown in Figure 6. The final EXAFS fit metrics are presented in Table 2.

MXAN Analysis. The MXAN analysis of the K edge of Cu(II) in aqueous ammonia began by again testing the most likely candidate structural models, starting with the best EXAFS-derived metrics from three different geometrical configurations: square, square pyramidal, and octahedral. The bond metrics and angular parameters that were fitted are detailed in the Materials and Methods section. In general, transverse atoms in both the equatorial and axial positions were metrically and geometrically linked, and transversely

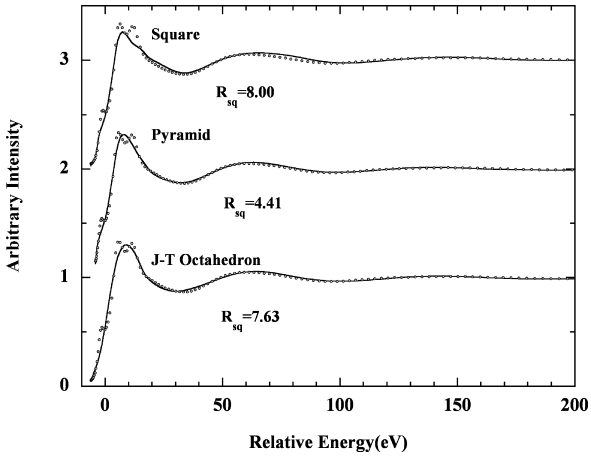

Figure 7. Copper K-edge XAS of 0.1 M Cu(II) in 4 M aqueous NH_3 (points) and MXAN fits (full lines) employing the following structural models: (top) $[Cu(NH_3)_4]^{2+}$ equatorial square, (middle) $[Cu(NH_3)_5]^{2+}$ axially elongated square pyramid, and (bottom) $[Cu(NH_3)_6]^{2+}$ Jahn−Teller distorted octahedron.

Table 3. Comparison of Primitive MXAN Structural Models[a]

	$N_{1,2eq}$	$\theta_{1,2}$	$N_{3,4eq}$	$\theta_{3,4}$	$N_{ax\text{-}up}$	$N_{ax\text{-}down}$	R_{sq}
square	1.96	89.5	1.97	90.5			8.00
pyramid	1.93	126.7	2.01	102.0	2.17		4.41
octahedron	1.93	108.6	1.97	71.4	2.09	2.09	7.63

[a] See the Materials and Methods section for definitions of the column headings.

conjoint out-of-plane migrations of the equatorial atoms were also allowed. All hydrogen atoms were included in the fits.

In Figure 7, the experimental data are compared with the calculated best fits for all three geometrical structures. The square pyramidal fit produced the lowest (best) goodness-of-fit R_{sq} value, indicating the best agreement between the theoretical calculation and the experimental data over the whole energy range. The metrics of the fits for all three geometries are summarized in Table 3. Although the square pyramidal geometry produced the best fit, the quality of this fit is poor in the low-energy region near 20 eV, where the XAS shows a split absorption maximum. This failure of the model indicated a need to enlarge the number of atoms used in the calculation, and the likelihood that a second shell of water contributed to the XAS spectrum, especially in the XANES energy region.

To evaluate a second shell, the same tetragonal, square pyramidal, and octahedral models were reconstructed. The first attempt included four water molecules positioned at the equatorial plane on lines bisecting the four equatorial N−Cu−N angles, as predicted by DFT.[36] In these tests of solvation, MXAN fits could not distinguish between second-shell waters or ammonias. Water was finally chosen to represent the second shell because of its mole-fraction excess. The initial second-shell Cu−O distance was set to be 2.80 Å, and the new fits floated the same structural parameters as previously used, plus the two new distances and two new polar angles that allowed positional adjustments of the second-shell atoms. Transverse atoms were always linked together, as before. During the fit, the four second shell waters iteratively migrated to their final best-fit positions.

These new fits showed substantial improvements in quality for both the square (R_{sq} = 3.69) and square pyramidal geometries (R_{sq} = 3.0), while octahedral fit was unimproved (R_{sq} = 7.72) (Supporting Information Figure S9). In all cases, the four second-shell waters migrated radially out from the starting 2.8 Å distance during the fits to the XAS spectrum, and the final best distances were all near 4 Å. The second-shell waters also migrated angularly out of the equatorial plane. Significantly, inclusion of the second shell improved the square and square pyramidal fits mainly in the low-energy range.

However, the best-integer second-shell EXAFS result included six waters rather than four waters. Therefore, the MXAN models were also expanded to test a second shell of six waters. In these fits, the MXAN fitting procedure was modified to provide more flexibility to the second shell while keeping the computation within reasonable limits. Thus, the best core ligand geometry derived from the four-water fits above was fixed during the six-water fits. The radial distance and two polar angles of each of the six second-shell waters were then allowed to float. In the starting six-water MXAN models, the second shell waters were distributed with a chemically rationalized asymmetry to take advantage of hydrogen bonding to the five ammonia ligands and a $-z$ axially localized water. Thus, four of the six second shell waters were initially situated near the centers of the four triangular faces of the $+z$ pentahedron capped by the axial ammonia and stationed at about H-bonding distance (2.9−3.1 Å) from at least one hydrogen of each of the five ammonia ligands (4 × Cu−O = 3.1 Å). The two remaining waters were initially situated at H-bonding distance on the $-z$ side of the complex ion (2 × Cu−O = 3.4 Å). When a $-z$ axial water was present, that is , in the J−T octahedral model, the set of two $-z$ second-shell waters resided on two adjoining faces of the $-z$ pentahedron capped by the axial water. These two second shell waters were distributed to be within H-bonding distance from each of the two hydrogens of the axial water and one of the equatorial ammonia ligands. In the tetragonal model, all six waters were within H-bonding distance of at least one equatorial ammonia ligand.

The results of these fits are shown in Table 4 and Supporting Information Figure S10. All three models showed very significant improvements, in contrast to the results from the four-water second-shell fits (compare Table 3 and Table 4). Most of the improvements again concentrated in the low-energy XANES region. The elongated square pyramidal model again produced the best overall fit, especially in the rising edge (−5−15 eV) and 100 eV energy regions relative to the fit with the octahedral model. The integrated areas of the absolute fit residuals, $fe(E)$ defined below, were 2.33 and 2.76 normalized area units, respectively. In the pyramidal model fit, the radial distances of the second shell $+z$ 4 × Cu−O waters increased by an average of 0.4 Å, while the two $-z$ waters shifted out about 0.2 Å, relative to the starting models. The $+z$ set of four waters also moved axially, with one transverse set of two moving further from and the second set of two moving closer to the equatorial plane.

Table 4. Primitive MXAN Models with Six Second-Shell Waters[a]

	first shell						second shell			
	$N_{1,2eq}$	$\theta_{1,2}$	$N_{3,4eq}$	$\theta_{3,4}$	N_{+z}	N_{-z}	$O_{1,2}$	$O_{3,4}$	$O_{5,6}$	R_{sq}
square + 2nd sh	1.94	86.6	2.01	102.1			3.0	3.4	3.6	3.44
pyramid + 2nd sh	1.97	79.4	2.00	84.1	2.93		3.3	3.3	4.0	2.76
octahedron + 2nd sh	1.94	104.8	1.94	104.8	2.18	2.18	3.0	3.0	3.3	4.16

[a] See the Materials and Methods section for definitions of the column headings.

Table 5. MXAN Fits to the Square Pyramidal Model with Added Second Shells[a]

	$N_{1,2eq}$	$\theta_{1,2}$	$N_{3,4eq}$	$\theta_{3,4}$	N_{ax}	O_{ax}	$O^{1-4}{}_{2sh}$	$O^{5,6}{}_{2sh}$	R_{sq}
pyramid	1.93	126.7	2.01	102.0	2.17				4.41
pyramid + ax water	1.94	101.7	1.97	122.0	2.16	3.67			4.01
pyramid + 2nd shell	1.97	79.4	2.00	84.1	2.93		3.3	4.0	2.76
pyramid + ax water + 2nd shell[b]	1.99	104.7	1.99	101.3	2.20	3.1	3.9 ± 0.2	3.6 ± 0.1	0.97

[a] Errors in the fitted values are ammonia ligand distances, equatorial $\pm$ (0.04 Å)$_{ste}$ $\pm$ (0.02 Å)$_{sys}$; axial $\pm$ (0.05 Å)$_{ste}$ $\pm$ (0.02 Å)$_{sys}$, axial long ($\pm$0.09 Å)$_{ste}$($\pm$0.02 Å)$_{sys}$, where ste represents the statistical error and sys represents the systematic error. [b] The average N_4 plane is $\theta = (103 \pm 1.7)°$, which is (0.45 $\pm$ 0.1) Å below the copper equatorial *xy* plane. Differences in the Cu$-N_{1,2eq}$ and Cu$-N_{3,4eq}$ distances are not significant for any of the fits except the pyramidal. The differences in polar angles are significant throughout, however. The plus/minus entries for the second shell oxygens in the final model are the standard deviations of the spread of individual distances and are in addition to the statistical and systematic uncertainties.

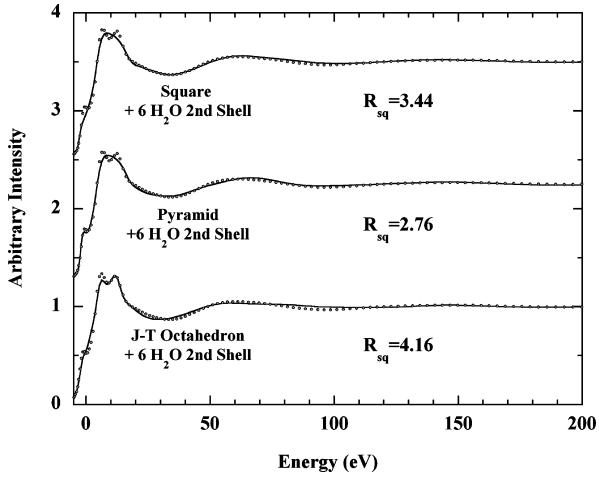

Figure 8. Copper K-edge XAS of 0.1 M Cu(II) in 4 M aqueous NH_3 (points) and MXAN fits (full lines) employing the same structural models as in Figure 7, now including a second shell of 6 water molecules. The split feature at the energy maximum near 10 eV in the octahedral fit reflects a scattering interaction between the axial ligands and the solvent shell, present also in the asymmetric model fit. Compare Figures 9c and 9d. The octahedral model did not fit the feature at 0 eV, however. See Supporting Information Figure 10 for this figure including *fe*(*E*) plots.

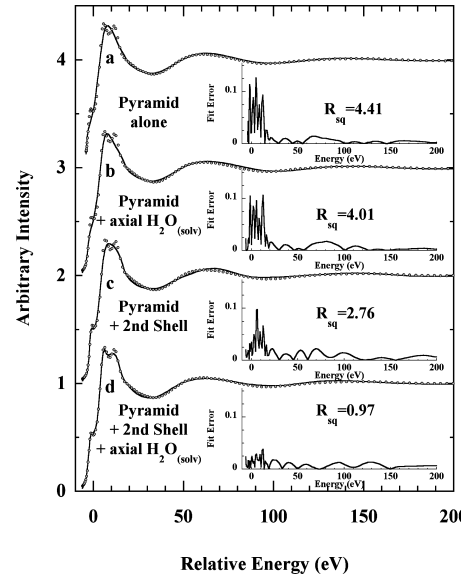

Figure 9. Copper K-edge XAS of 0.1 M Cu(II) in 4 M aqueous NH_3 (points) and the MXAN fits (full lines) using the $[Cu(NH_3)_5]^{2+}$ model: (a) square pyramid alone; (b) panel a plus an axial water; (c) panel a plus six solvent waters; (d) panel a plus panel b plus panel c. Insets: the fit error function *fe*(*E*), (see text), indicating the unfit residual; all plotted to the same scale. The improvement in the fit is found primarily in the rising edge energy region of the XAS spectrum.

The MXAN model was finally expanded to determine whether the square pyramidal geometry might be augmented with a $-z$ axially solvating water molecule at ~2.8 Å, as found in the EXAFS analysis. The addition of this structural feature greatly improved the fit, reducing R_{sq} by nearly two full units, from 2.76 to 0.97. For the final two fits, the inner six-molecule core of the axially dissymmetric model was fixed at the $R_{sq} = 2.76$ positions. The three sets of two second-shell waters and the long axial water were allowed to float to their best positions ($R_{sq} = 1.09$). The second shell of six plus one waters was then fixed, and the inner ligand core was floated to the final best positions ($R_{sq} = 0.97$). The final MXAN structural arrangement is entirely consistent with the axially dissymmetric model found by EXAFS analysis.

Figure 9 shows the results from the fits to the set of increasingly complete square pyramidal models. These are displayed in stepwise fashion to show how the XAS spectrum is built up from the increasing scattering profile. Figure 9a shows the bare square pyramidal fit, and Figure 9b is the result of adding a $-z$ axial water at 2.8 Å. For this structure, substitution of a distant solvating axial ammonia for the 2.8 Å water produced a slightly poorer fit ($R_{sq} = 4.26$, Cu$-N_{ax} = 2.6$ Å). Figure 9c shows the square pyramid with six ~3.8 Å second-shell waters.

Finally, Figure 9d shows the complete best MXAN model for Cu(II) in aqueous ammonia. This consisted of an axially elongated square pyramid including a transverse axially localized water 3.1 Å below the equatorial plane, and a second shell of six water molecules near 3.8 Å. All ammonia and water hydrogens were included in this fit. The goodness-of-fit $R_{sq} = 0.97$ is almost 3-fold better than that for the pure square pyramidal geometry with a second shell of six 3.8 Å waters alone (Table 4). Close examination of Figure 9d reveals that the strong shoulder at 0 eV on the XAS rising edge was well-fit only when the 3.1 Å axial solvent and the 3.8 Å second shell were both present. This finding directly

illustrates the important contribution made by distant organized scatterers to the structure of the rising K-edge of an X-ray absorption spectrum. This topic will be discussed further below.

To visualize the detailed behavior of the error over the whole energy range, the fit error is shown as a function of energy in the Figure 9 insets. This error, defined as

$$fe(E) = \sqrt{(y^i_{th}(E) - y^i_{exp}(E))^2}$$

gives a clear indication of the goodness-of-fit over the whole energy range. From Figure 9a to d, an especially large decrease of $fe(E)$ is noted in the rising edge energy region. This behavior corresponds to a substantial building of the total photoabsorption cross section as a function of the number of atoms around the absorber, and directly illustrates the effect of distant scatterers on the lower energy portion of a K-edge XAS spectrum. The metrics related to the build-up of the final axially dissymmetric model are summarized in Table 5.

The equatorial ligands are notably well defined throughout the model series and remained in a coherent geometrical array. These ligands made the strongest contribution to the EXAFS region of the XAS spectrum, indicated by the relatively small model sensitivity of $fe(E)$ above 100 eV. The axial atoms were much more variable, showing a distinct sensitivity to second-shell solvation (Tables 3−5). Their contributions to the total cross section are principally restricted to the low-energy part of the spectrum, well-reflected in $fe(E)$. This is a clear indication that the atoms in the equatorial plane dominate the total XAS signal. This situation is quite common and was found in the analysis of Cu(II) in water[37,38] and of the Fe K-edge of heme-like compounds.[10,39]

Discussion

Although the EXAFS fits favor the dissymmetric square pyramidal model over the elongated octahedral model, this preference is more indicative than definitive. However, the MXAN analysis was very clear in excluding the octahedral model in favor of the square pyramidal model (Figure 8). EXAFS and MXAN fitting experiments represent different approaches to obtaining structural metrics from XAS spectra. At least part of the more definitive model preference attending the MXAN fits is that this approach uniquely includes the geometrical information in the rising K-edge energy region. Applying both EXAFS and MXAN analysis to single data sets takes advantage of the peculiar strengths each approach and provides a relatively independent cross-check on the derived structural models.

The improved MXAN fits resulting from the added second shells were not an artifact of increased degrees of freedom. Multiple scattering is angle and distance dependent, and additional distant waters will produce new scattering signals that can make a fit worse rather than better. It is also important to note that the final distances and angles of the second-shell waters were not arbitrary. These parameters were iteratively adjusted during the MXAN fit to minimize the fit residual, R_{sq}, as indicated by the systematic shifts of the second-shell waters from their starting positions to the final distribution around the core copper−ligand complex. The distances and angles are therefore not fortuitous but instead constrained by the calculated match to the data. The square pyramidal core geometry always produced the best agreement with the experimental data, indicating the preferred geometrical arrangement around Cu(II).

In the comparison of EXAFS and MXAN fits, it is important to recognize that the accounting of single- and multiple-scattering interactions by EXAFS analysis is restricted to the continuum energy region of an XAS spectrum. In contrast, MXAN analysis always evaluates the entire XAS spectrum, including both the continuum region and the classically bound-state rising edge energy region.[8,10,11] In addition, MXAN specifically includes the full absorber−scatterer angular relationships (i.e., both polar angles), whereas pure EXAFS analysis is restricted to radial distributions. The structural models derived from these two methods can therefore differ in detail, (compare Tables 2 and 5) because the data sets and model constraints are never entirely comparable. For its part, EXAFS analysis is computationally less demanding and allows more rapid testing of alternative structural models. In this event, the final EXAFS and MXAN models for Cu(II) in aqueous ammonia solution are indistinguishable within 2 standard deviations (SD) in the long axial solvent distance and to less than 1 SD in the equatorial and axial ligand distances. The only major structural difference resides in the distance to the second-shell scatterers. This difference likely is because the EXAFS fit does not include the full absorber−scatterer information resident in the rising edge energy region, as noted above. Nevertheless, the EXAFS and MXAN approaches independently, that is, referenced only to goodness-of-fit, produced virtually identical structural outcomes.

The MXAN model further showed that the equatorial ammonias about Cu(II) are uniformly displaced about (13 ± 1.7)° below the equatorial plane of copper. Although the magnitude of these angles proved model-dependent (Table 5), the ∼−13° bend marks a distinction with the transverse +5°, −17° distorted D_{2d}-like arrangement of equatorial waters found to characterize $[Cu(H_2O)_5]^{2+}$.[38,40]

The unique strength of the MXAN formulation is that the multiple-scattering (MS) theoretical approach allows a complete recovery of both the bound and continuum states of a large variety of molecular systems, all within a single coherent one-electron physical theory.[6,41] This extended

(37) Benfatto, M.; D'Angelo, P.; Della Longa, S.; Pavel, N. V. *Phys. Rev. B* **2002**, *65* (174205), 1–5.
(38) Frank, P.; Benfatto, M.; Szilagyi, R. K.; D'Angelo, P.; Della Longa, S.; Hodgson, K. O. *Inorg. Chem.* **2005**, *44*, 1922–1933.
(39) Della Longa, S.; Arcovito, A.; Girasole, M.; Hazemann, J. L.; Benfatto, M. *Phys. Rev. Lett.* **2001**, *87* (155501), 1–4.
(40) Frank, P.; Benfatto, M.; Szilagyi, R. K.; D'Angelo, P.; Della Longa, S.; Hodgson, K. O. *Inorg. Chem.* **2007**, *46*, 7684–7684.
(41) Johnson, K. E. Scattered-Wave Theory of the Chemical Bond. In *Advances in Quantum Chemistry*; Löwdin, P.-O., Ed.; Academic Press: New York, 1973; Vol. *7*, pp 143−185.

continuum approach,[42] treats the bound states as very narrow scattering resonances located above the muffin-tin interstitial potential, V_{mt}, permitting the bound-state transitions to be calibrated with the continuum features on the same energy scale without the need to calculate the ionization energy.

The total absorbing cross section can be written in terms of the scattering path operator,[8,42] τ, defined as $\tau = (T_a^{-1} + G)^{-1}$, where $(T_a^{-1})^{ij}_{L,L'} = [(t^i_l)^{-1}]\delta_{ij}\delta_{L,L'}$, and where t^i_l are the atomic scattering amplitudes defined in terms of phase shift and G are the free electron propagators. It turns out that the modulus of the free electron propagators behaves as $|G| \approx 1/(kR)$, where k is the photoelectron wave vector defined as $k = (E - V_{mt})^{1/2}$ and R is the interatomic distance. This $1/(kR)$ dependence can be significant when k is small and R is large, meaning that multiple scattering resonances from distant atoms can appear at energies as low as the immediate rising K-edge. Likewise the mean free path of the photoelectron is very large (~7−10 Å) at low energies.[43] This means at low energies the photoelectron probes distant atoms, which again points to the fact that atoms far from the absorber can contribute to the low-energy rising edge part of the XAS spectrum. The $1/(kR)$ and mean free-path dependencies of multiple scattering phenomena lead to the classically counterintuitive prediction that resonances from interactions with distant scatterers will appear at photoelectron energies well below the ionization energy.[8,11,42,44,45] Examples of this are evident in Figure 9c and d, where strong rising edge features at 11 and ~0 eV, respectively, are explained only with the addition of distant atom shells that are neither directly bonded to the central copper ion nor covalently linked to ligand atoms. Thus, the better fit upon addition of distant scatterers occurs in part because the relatively low-energy photoelectron produced in the rising edge energy region has a long mean-free path and can scatter from distant atoms,[8,11,43] which thereby contribute to the structure of the XAS rising edge. In this event, some low-energy rising edge features that might otherwise be described as many-body bound-state shakedown transitions[46–52] could instead, in whole or in part, be caused by single-electron scattering from distant atoms. This possibility should always be tested in evaluating features that occur on the rising edges of transition metal XAS spectra and is likely to affect assessments of metal−ligand covalency.[48,50,51]

It was expected at the outset of this work that the similarity of the H_2O and H_3N molecules ensured that aqueous ammonia would constitute the next-most-simple solution milieu for Cu(II) after water alone. Thus, Cu(II) in aqueous ammonia was naively expected to inhabit a structural environment comparable to that in pure water solution. However, the anticipated structural simile did not follow, and this disparity is discussed further below.

The equilibrium composition of the solution (Figure S1 in the Supporting Information) requires that about 32% of the pyramidal Cu(II) complexes should include an apical water molecule. In the crystal structures of the two majority equilibrium solution complexes, the axial NH_3 or H_2O bond lengths are 2.19 and 2.34 Å, respectively. If these distances were preserved in the two solution equilibrium structures, then the EXAFS data will have included scattering waves reflecting each distance. The best EXAFS fit using only a single axial ligand would then have produced a single weighted average distance with a high Debye−Waller factor because partial occupancies at two different distances would have had an effect on the EXAFS fit similar to static disorder in the distance to a single scatterer. Table S1 shows that the axial ligand DW-factor is indeed quite large, and the data in Figure 3 show that the systematic error of the axial ligand distance is also large (±0.06 Å at $\Delta F = 1$).[53]

To test whether the calculated equilibrium solution composition could be reproduced by an EXAFS model with a fractional mixture of axial ligands, fits with noninteger axial ligand coordination numbers were carried out. For example, a core square pyramidal fit with two axial occupancies, of coordination number (CN) 0.35 and 0.65, could reflect the equilibrium-fractional occupancies of water and ammonia ligands, respectively. Indeed a reasonable fit was obtained using this model, (e.g., $F = 0.1407$), and the axial distances bifurcated to 2.16 Å, DW = 0.00131 and 2.31 Å, DW = 0.00080, for occupancies of CN = 0.65 and 0.35, respectively. When the square pyramidal model was then expanded to include a long -z axial scatterer, the fitted axial distances were CN = 0.65 at 2.14 Å, DW = 0.00218, CN = 0.35 at 2.30 Å, DW = 0.00165, and CN = 1.0 at 2.78 Å, DW = 0.00875 ($F = 0.1047$). This drop of nearly four units in F-value following addition of a single-scattering path is more than can be accounted for by two increased degrees of freedom alone. The axially noninteger fits are shown in Figure S8 in the Supporting Information. The degrees of freedom in this fit (15 variables) do not exceed the number of statistically independent data points (24), and so the data are not overfit. When the path occupancies were reversed, the CN = 0.35 axial occupancy, now at 2.12 Å, produced a physically meaningless DW = −0.0006. Thus, the fit using the partial occupancies predicted by the equilibrium distribution (Figure S1 in the Supporting Information) produced nearly the same distances as found in the crystal structure of $[Cu(NH_3)_5]^{2+}$ and $[Cu(NH_3)_4(H_2O)]^{2+}$, respectively. At the

(42) Tyson, T. A.; Hodgson, K. O.; Natoli, C. R.; Benfatto, M. *Phys. Rev. B* **1992**, *46*, 5997–6019.
(43) Müller, J. E.; Jepsen, O.; Wilkins, J. W. *Solid State Commun.* **1982**, *42*, 365–368.
(44) Strange, R. W.; Alagna, L.; Durham, P.; Hasnain, S. S. *J. Am. Chem. Soc.* **1990**, *112*, 4265–4268.
(45) Bocharov, S.; Kirchner, T.; Drager, G.; Šipr, O.; Šimunek, A. *Phys. Rev. B* **2001**, 63 (045104), 1–10.
(46) Bair, R. A.; Goddard, W. A., III *Phys. Rev. B* **1980**, *22*, 2767–2776.
(47) Wirt, M. D.; Sagi, I.; Chen, E.; Frisbie, S. M.; Lee, R.; Chance, M. R. *J. Am. Chem. Soc.* **1991**, *113*, 5299–5304.
(48) Shadle, S. E.; Penner-Hahn, J. E.; Schugar, H. J.; Hedman, B.; Hodgson, K. O.; Solomon, E. I. *J. Am. Chem. Soc.* **1993**, *115*, 767–776.
(49) Kim, M. G.; Cho, H. S.; Yo, C. H. *J. Phys. Chem. Solids* **1998**, *59*, 1369–1381.
(50) DuBois, J. L.; Mukherjee, P.; Stack, T. D. P.; Hedman, B.; Solomon, E. I.; Hodgson, K. O. *J. Am. Chem. Soc.* **2000**, *122*, 5775–5787.
(51) Horne, C. R.; Bergmann, U.; Grush, M. M.; Perera, R. C. C.; Ederer, D. L.; Callcott, T. A.; Cairns, E. J.; Cramer, S. P. *J. Phys. Chem. B* **2000**, *104*, 9587–9596.
(52) Chaboy, J.; Munoz-Paez, A.; Carrera, F.; Merkling, P.; Marcos, E. S. *Phys. Rev. B* **2005**, *72* (134208), 1–7.
(53) Michalowicz, A.; Provost, K.; Laruelle, S.; Mimouni, A.; Vlaic, G. *J. Synchrotron Rad.* **1999**, *6*, 233–235.

same time, the axial DW-values took on reasonable values and the improvement following addition of the long axial solvent scatterer remained evident. On the basis of equilibrium chemistry, the CN = 0.65 scatterer is assigned to ammonia, and therefore, the CN = 0.35 scatterer to water. The relatively high DW-value of the 2.16 Å axial path in the final EXAFS fit, Table 2, and of the 2.19 Å path in the EXAFS fit using the pure square pyramidal model, Table S1, can then be explained as most likely reflecting a partial axial occupancy divided between ammonia and water ligands residing at two different distances.

A straightforward interpretation of all these results is that the solution structure of Cu(II) in aqueous ammonia solution includes four equatorial ammonia ligands plus an equilibrium proportioned mixture of ammonia and water sharing axial ligation in a core geometry consisting of an elongated square pyramid. Each of the partial occupancy axial ligands resides at a separate distance as predicted by the crystal structure models and the K_5 equilibrium constant. Along with the core square pyramidal geometry, a single strongly localized solvent molecule occupies the $-z$ axial side of copper. Both the EXAFS and the MXAN analyses also discerned a second shell of six solvent molecules, which may be water, or ammonia, or a mixture of both.

An axially localized solvent molecule near 3 Å has a certain ambiguity with respect to structure. It is not a ligand, nor is it part of the surrounding solvation shell that bridges the phase-change from complex ion to bulk solvent. However, a description of Cu(II) in 4 M aqueous ammonia would be incomplete without the 3 Å axial scatterer, which may perhaps be best described as a solvent molecule strongly localized by virtue of a specific charge−dipole interaction that is available only along the $-z$-axis of both $[Cu(NH_3)_5]^{2+}$ and $[Cu(NH_3)_4(H_2O)]^{2+}$. This situation may perhaps be notationally represented, for the majority complex of Cu(II) in ammonia, as $\{[Cu(NH_3)_5](solv)\}^{2+}$, where use of "solv" acknowledges the ambiguity in the identity of the axial scatterer. With the second shell of solvent molecules, the entire extended complex might be represented as $\{[Cu(NH_3)_5](solv)\}^{2+}\cdot 6solv$.

For the solvent shell to achieve the durability revealed by the strong contribution to the XAS rising K-edge, the lifetime of the solvated complex should reasonably be ≥100 times longer than the rotational correlation time of the complex ion. This lifetime is not known for Cu(II) in ammonia solution, but for Cu(II) in water, it is 0.7×10^9 s^{-1}.[54] Thus the entire complex $\{[Cu(NH_3)_5](solv)\}^{2+}$ complex should have an equilibrium lifetime of $\geq 10^{-7}$ s. This minimal value is about 30% of the dissociation lifetime of the tetraammine complex itself, ($\sim 3 \times 10^{-7}$ s).[55] Indeed, to make so strong a contribution to the copper K-edge XAS spectrum as it does, the entire $\{[Cu(NH_3)_4L](solv)\}^{2+}\cdot 6solv$ complex (L = NH_3, H_2O) must represent the predominantly stable average structure in 4 M aqueous ammonia solution.

The ligand exchange rate for $[Cu(H_2O)_5]^{2+}$ in water is about 1000 times faster than that for $[Cu(NH_3)_5]^{2+}$ in aqueous ammonia,[54,55] which also implies a more stable second-shell solvation environment in the ammonia complex. Thus, Nagypál, et al., reported[55] that the paramagnetic relaxation time (T_{2B}) of $[Cu(NH_3)_5]^{2+}$ was much larger than that for $[Cu(NH_3)_4(H_2O)]^{2+}$, further noting this implied a change of geometry when the fifth ammonia became liganded. In view of the finding that solution-phase $[Cu(H_2O)_5]^{2+}$, $[Cu(NH_3)_4(H_2O)]^{2+}$, and $[Cu(NH_3)_5]^{2+}$ are all square pyramidal, the geometric change about Cu(II) proposed by Nagypál, et al., could not be in the first shell. Considering the durable second shell uniquely present around $[Cu(amm)]^{2+}$, it seems likely that the geometric effect noted by Nagypál, et al. resides in a second shell that may be especially stabilized when the fifth ammonia is present. This is discussed further below.

Figure 10 shows a structural cartoon of the final model for Cu(II) in aqueous ammonia solution, including the ~3.8 Å solvent shell reflecting the metrics derived from the MXAN fit (Table 5). Figure 10 insets show that the $\Delta R_{sq} = \pm 1$ dependence of the axial ligand distance and the axial solvent distance are −0.14/+0.22 and −0.10/+0.17 Å, respectively. These broad minima are suggestive that neither the axial ligand nor the axial solvent can be fully represented by a single distance. The R_{sq} minima for the 2.35 Å axially liganding water in square pyramidal $[Cu(H_2O)_5]^{2+}$ was much broader and exceptionally asymmetric, tailing off at axial bond distances greater than 2.6 Å, with $\Delta R_{sq} = \pm 1$ yielding $-0.2/+\geq 0.3$ Å. In this case, the impact of increasing axial ligand distance on R_{sq} became small, indicating the insensitivity of the fit to further increases in axial water distance. This means scattering interactions from waters at distances of >2.65 Å are insignificantly small in the copper K-edge XAS spectrum of aqueous $[Cu(H_2O)_5]^{2+}$, signifying disorganization of the solvent shell. The case of $[Cu(amm)]^{2+}$ was in striking contrast, wherein R_{sq} continued to increase with both axial and second-shell solvent distances. This interesting disparity in sensitivity appears because the XAS data for Cu(II) in 4 M aqueous ammonia contains elements reflecting active scatter of the photoelectron by durably organized molecules at long distances. Thus, molecules incorrectly placed in the model, even at long distances from the copper ion, will continue to decohere the calculated XAS from the measured XAS. This is not the case for the known XAS of Cu(II) in water, which shows no evidence for scatterers at distances beyond the axial ligand. This result indicates that the solvent shell around $[Cu(NH_3)_5]^{2+}$ is much more tightly organized than the solvent around $[Cu(H_2O)_5]^{2+}$. This point is discussed further below.

The structure of Cu(II) in aqueous ammonia solution has been the subject of other studies. In the earliest EXAFS investigation, Sano, et al.[56] could not find a signal for the axial ligand. However, their data were consistent with a square pyramidal geometry, although the axial ligand assignment was based only on electronic spectroscopy. Monte Carlo simulations have been used to determine the range of structures, and their distributions, for Cu(II) in water solution

(54) Poupko, R.; Luz, Z. *J. Chem. Phys.* **1972**, *57*, 3311–3318.
(55) Nagypál, I.; Debreczeni, F. *Inorg. Chim. Acta* **1984**, *81*, 69–74.
(56) Sano, M.; Maruo, T.; Masuda, Y.; Yamatera, H. *Inorg. Chem.* **1984**, *23*, 4466–4469.

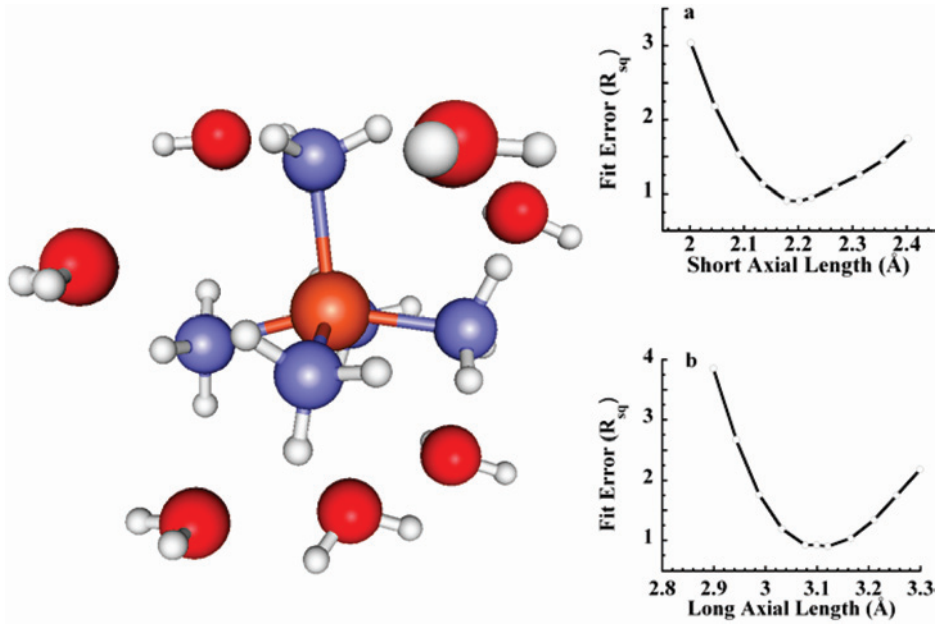

Figure 10. Cu(II) in aqueous ammonia, showing the MXAN final model, including the nonbonded axial water at 3.1 Å and the six solvent−waters near ~3.8 Å. Insets: The R_{sq} dependence on distance to copper from (a) the axial ammonia and (b) the 3.1 Å water. See the Supporting Information for CuN-6w-8-best.MOL, representing the $\{[Cu(NH_3)_5(H_2O)\}^{2+}\cdot 6H_2O$ structural model.

with a variety of ammonia concentrations.[57–59] These studies, while interesting, did not reproduce the known equilibrium composition for the experimental solution conditions and invariably predicted octahedral structures rather than square pyramidal. Among other things, these experiments illustrate the hazards of calculations from theory that are unconstrained by known experimental results.

Alternatively, calculations from gas-phase DFT predicted that 4-coordinate $[Cu(NH_3)_4]^{2+}$ is the stable structure for Cu(II) in aqueous ammonia.[36,60] Although, the relevance of these studies to the solution-phase structure is ambiguous, one of them[36] also implicated a specific solvation array as part of the final Cu(II)-ammonia structure. This core plus second-shell structure can be thought of as the base complex from which the final solvated pyramidal geometry emerges when the full impact of removal to solution-phase aqueous ammonia is present.

Recently, Nilsson, et al.[28] reported that EXAFS analysis of Cu(II) in liquid and aqueous ammonia yielded a Jahn−Teller distorted octahedral model with $4 \times N_{eq}$ at 2.023(5) Å and $2 \times N_{ax}$ at 2.78(5) Å. This model is statistically indistinguishable from the long-axial J−T octahedral model discussed here (Table S1 in the Supporting Information). The J−T octahedron model is in many respects similar to the final axially solvated square pyramidal model, in that adjusting only one of the axial ligands to 2.16 Å would bring the two core models into complete consonance (see also Table S2 and Figures S5 and S6 in the Supporting Information).

The most ambitious prior analysis of the structure of Cu(II) in aqueous ammonia also used the MXAN method to model the copper K-edge XAS spectrum.[19,52,61] In a striking confluence with the results reported here, this study reported that the rising edge feature near 0 eV (Figure 9) was reproduced with the addition of distant solvent−waters to the structural model. However, this discovery was not pursued. Instead, the 0 eV shoulder was interpreted as arising from the tetragonal distortion of an octahedral structure, and the feature at 11 eV was explained in terms of a double excitation "shakedown" transition. Recourse to this explanation, however, followed from an analysis restricted to a fixed tetragonal geometry for $[Cu(NH_3)_4]^{2+}$ or a fixed J-T distorted octahedron for $[Cu(NH_3)_4(H_2O)_2]^{2+}$. No other geometries were tested. The lack of success with these models actually corroborates the fitting experiments reported here, which found each of these geometric models to be an inadequate description of the structure of Cu(II) in aqueous ammonia. Greater exploration of the structural space showed that the rising K-edge features can arise largely from interactions of the photoelectron with distant nonbonded atoms, as predicted by the $1/kR$ and mean free path dependencies of the photoelectron. The MXAN results reported here thus also show the importance of opening bond angles and metal−ligand distances during a structural fit to XAS data to allow the appropriate interplay between the target experimental XAS spectrum and the theoretical description.

Finally, the perplexing difference between the structure of Cu(II) in aqueous ammonia solution relative to that of Cu(II) in water solution, when the media are ostensibly so similar, is considered. In exploring this question, the axially dissymmetric solvated model for Cu(II) in aqueous ammonia solution was tested against the XAS data for Cu(II) in water solution.[37,38] The preliminary result, to be reported in detail

(57) Pranowo, H. D.; Rode, B. M. *J. Chem. Phys.* **2000**, *112*, 4212–4215.
(58) Pranowo, H. D.; Rode, B. M. *Chem. Phys.* **2001**, *263*, 1–6.
(59) Pranowo, H. D. *Chem. Phys.* **2003**, *291*, 153–159.
(60) Pavelka, M.; Burda, J. V. *Chem. Phys.* **2005**, *312*, 193–204.
(61) Chaboy, J.; Muñoz-Paez, A.; Merkling, P. J.; Marcos, E. S. *J. Chem. Phys.* **2006**, *124* (064509), 1–9.

elsewhere, was that the model for Cu(II) in aqueous ammonia solution was completely unable to fit the K-edge XAS spectrum for Cu(II) in pure water solution. The XAS data presently in hand for Cu(II) in water, for example, could not support an axially localized ~3 Å solvent molecule. Nor was any need found to include a second shell of solvent molecules. In a global sense the two structures are similar only in that the core ligation sphere about Cu(II) is an elongated square pyramid.

For $[Cu(amm)]^{2+}$ in aqueous ammonia, a possible organizing force for localization of the second shell could stem from the extra hydrogen bond that the ammonia molecule can support. A look at Figure 10 shows that there is no ammonia rotamer without at least one hydrogen above and below the equatorial N_4 plane. An H-bonding network can be envisioned that is stable to Cu−N rotation of the ammonia ligands, thus positioning the second-shell solvent atoms with respect to the central copper. Fixed in an equilibrium sense, these second shell molecules could produce multiple scattering features in a K-edge XAS spectrum. Including the axial ammonia, five ammonia ligands may thus be able to organize a solvent molecule on each of the four $+z$ faces of a square pyramid. This possibility is not available to Cu(II) with five water ligands because the H-bond direction of liganding water is disorganized by equatorial Cu−O rotation.

In addition, the $-z$ axially localized solvent molecule in aqueous ammoniacal $\{[Cu(NH_3)_5](solv)\}^{2+}$ is about 2.6 Å from the hydrogen atoms of the equatorial ammonia ligands, and about 3.2 Å from the ammonia nitrogens. These distances are consistent with a weak hydrogen bond.[62–65] It seems conceivable that the forces localizing this axial solvent molecule include multiple H-bonding interactions between the solvating oxygen or nitrogen lone pair and four hydrogens of the equatorial ammonia ligands, as well as the charge on copper. So fixed, this $-z$-axial solvent molecule may then help to partially stabilize the positions of the two second-shell solvent molecules modeled on the $-z$ faces of the axially dissymmetric complex ion. This idea could be converted to a quantitative hypothesis by the application of computational theory.[65,66] Residual K-edge intensity that could not be fit using an experimentally resolved solvent sphere might warrant explanation as a double-electron shake-down transition. However, resort to this explanation should only follow exhaustion of all structural possibilities supported by single-electron theory.[67]

The distorted square pyramid has now been found to be the distinctly preferred structural motif for Cu(II) in both water and in aqueous ammonia. While the ligand geometry of Cu(II) in ammonia apparently lacks the distorted D_{2d}-like equatorial displacements of $[Cu(H_2O)_5]^{2+}$, the copper ion in the equilibrium $[Cu(amm)]^{2+}$ core structure is about 0.45 ± 0.1 Å above the equatorial N_4 plane (Table 5). This distance is entirely comparable to the out-of-plane displacement of biological copper observed in the active sites of blue copper proteins.[68–70] The classic pseudotetrahedral $2N_{His}S_{Cys}S_{Met}$ copper site geometries of azurin and plastocyanin[71,72] are distorted away from the canonical Jahn−Teller axially elongated octahedron of crystalline Cu(II).[70] Since the early hypothesis of Malmstrom[73] and Vallee and Williams,[74] standard practice has been to explain this distortion as imposed by a stiff protein rack.[75–80] A hydrogen-bonding network has been proposed as the structural framework of this rack-enforced copper-site geometry.[78,79,81] Rack-induced bonding has already been opposed on calculational grounds.[82–84] However, the ~20−70 kJ of exothermic folding free energy that stabilizes native proteins[85] is insufficient to support any appreciable added endothermic strain. The profound motional dynamics of native proteins, which produce kinetically labile populations of structural substates, support the same negative conclusion regarding protein rigidity.[86–94] Thus, ~20−70

(62) Wallwork, S. S. *Acta Crystallogr.* **1962**, *15*, 758–759.
(63) Lakshmi, B.; Samuelson, A. G.; Jose, K. V. J.; Gadre, S. R.; Arunan, E. *New J. Chem.* **2005**, *29*, 371–377.
(64) Harris, T. K.; Mildva, A. S. *Prot. Struct. Funct. Genet.* **1999**, *35*, 275–282.
(65) Grabowski, S. J. *J. Phys. Org. Chem.* **2004**, *17*, 18–31.
(66) Ranganathan, A.; Kulkarni, G. U.; Rao, C. N. R. *J. Phys. Chem. A* **2003**, *107*, 6073–6081.
(67) Ockham, W. of In *The Encyclopedia of Philosophy*; Edwards, P., Ed.; Macmillan and the Free Press: New York, 1972 (1495); Vol. *8*, pp 307.
(68) Andrew, C. R.; Yeom, H.; Valentine, J. S.; Karlsson, B. G.; Bonander, N.; van Pouderoyen, G.; Canters, G. W.; Loehr, T. M.; Sanders-Loehr, J. *J. Am. Chem. Soc.* **1994**, *116*, 11489–11498.
(69) Hart, P. J.; Nersissian, A. M.; Herrmann, R. G.; Nalbadyan, R. M.; Valentine, J. S.; Eisenberg, D. *Protein Sci.* **1996**, *5*, 2175–2183.
(70) Messerschmidt, A. Metal Sites in Small Blue Copper Proteins, Blue Copper Oxidases and Vanadium-Containing Enzymes. In *Structure and Bonding*; Springer Verlag: Berlin, 1998; Vol. *90*, pp 37−68.
(71) Adman, E. T.; Jensen, L. H. *Isr. J.Chem.* **1981**, *21*, 8–13.
(72) Guss, J. M.; Freeman, H. C. *J. Mol. Biol.* **1983**, *169*, 521–563.
(73) Malmstrom, B. G. Two forms of copper in copper-containing oxidases. In *Oxidases and Related Redox Systems*; King, T. E., Mason, H. S. and Morrison, M., Ed.; Wiley: New York, 1964; Vol. *1*, pp 207−216.
(74) Vallee, B. L.; Williams, R. J. P. *Proc. Natl. Acad. Sci. U.S.A.* **1968**, *59*, 498–505.
(75) Karlsson, B. G.; Aasa, R.; Malmström, B. G.; Lundberg, L. G. *FEBS Lett.* **1989**, *253*, 99–102.
(76) Malmström, B. G. *Eur. J. Biochem.* **1994**, *223*, 711–718.
(77) Solomon, E. I.; LaCroix, L. B.; Randall, D. W. *Pure Appl. Chem.* **1998**, *70*, 799–808.
(78) Gray, H. B.; Malmström, B. G.; Williams, R. J. P. *J. Biol. Inorg. Chem.* **2000**, *5*, 551–559.
(79) Machezynski, M. C.; Gray, H. B.; Richards, J. H. *J. Inorg. Biochem.* **2002**, *88*, 375–380.
(80) Zong, C. H.; Wilson, C. J.; Shen, T. Y.; Wittung-Stafshede, P.; Mayo, S. L.; Wolynes, P. G. *Proc. Natl. Acad. Sci. U.S.A.* **2007**, *104*, 3159–3164.
(81) Dong, S. L.; Ybe, J. A.; Hecht, M. H.; Spiro, T. G. *Biochemistry* **1999**, *38*, 3379–3385.
(82) Dorfman, J. R.; Bereman, R. D.; Whangbo, M.-H. Utilization of Pseudo-Tetrahedral Copper(II) Coordination Compounds to Interpret the Stereoelectronic Properties of Type I Copper(II) Centers in Metalloproteins. In *Copper Coordination Chemistry: Biochemical and Inorganic Perspectives*; Karlin, K. D., Zubieta, J., Ed.; Adenine: Guilderland, NY, 1983, pp 75−96.
(83) Ryde, U.; Olsson, M. H. M.; Pierloot, K.; Roos, B. O. *J. Mol. Biol.* **1996**, *261*, 586–596.
(84) Ryde, U.; Olsson, M. H. M. *Intl. J. Quant. Chem.* **2001**, *81*, 335–347.
(85) Liu, L.; Yang, C.; Guo, Q. X. *Biophys. Chem.* **2000**, *84*, 239–251.
(86) Frauenfelder, H.; Sligar, S. G.; Wolynes, P. G. *Science* **1991**, *254*, 1598–1603.
(87) Tang, K. E. S.; Dill, K. A. *Intl. J. Quant. Chem.* **1999**, *75*, 147–164.
(88) Wand, A. J. *Nat. Struct. Biol.* **2001**, *8*, 926–931.
(89) Vendruscolo, M.; Paci, E.; Dobson, C. M.; Martin Karplus, M. *J. Am. Chem. Soc.* **2003**, *125*, 15686–15687.
(90) Fenimore, P. W.; Frauenfelder, H.; McMahon, B. H.; Young, R. D. *Proc. Natl. Acad. Sci. U.S.A.* **2004**, *101*, 14408–14413.
(91) Hill, J. J.; Shalaev, E. Y.; Zografi, G. *J. Pharm. Sci.* **2005**, *94*, 1636–1667.

kJ of net thermodynamic stability in folded native proteins, including blue copper proteins,[38,95,96] cannot support 30−70 kJ[76,97,98] of unfavorable geometric strain asymmetry on the oxidized blue copper site, and thus cannot provide a rigidly imposed endergonic protein rack. The proposed endergonic rack-bonding strain energy is enough to neutralize the free energy of folding and cause blue copper proteins to spontaneously denature.[38] That blue copper proteins do not spontaneously denature empirically testifies to the absence of any significant endothermic rack strain.

A protein rack is also structurally superfluous to an explanation of the blue copper site geometry because unconstrained Cu(II) in water solution, $[Cu(H_2O)_5]^{2+}$, is already a tetragonally distorted square pyramid,[37,38,99] as is Cu(II) in 4 M aqueous ammonia, $[Cu(amm)]^{2+}$ but now with copper raised ∼0.45 Å above the depressed N_4 plane.

By merely replacing two equatorial ammonia ligands of $[Cu(NH_3)_5]^{2+}$ with one short sulfur thiolate ligand, and with no other change, a reasonable $[CuN_3SR]^+$ geometrical facsimile of the blue copper site of oxidized Plastocyanin or Azurin is obtained.[69,100–103] All the biomimetic asymmetry of this blue copper facsimile is already present in the unconstrained solution $[Cu(NH_3)_5]^{2+}$ complex ion and so would have no need for a rack-induced enforcement.[38,82,104,105] The only apparent instability of an unconstrained pseudotetrahedral $[Cu(N_3SR)]^+$ center is chemical, namely, the redox-mediated bimolecular decomposition to Cu(I) plus disulfide.

Finally, it seems certain that when in unconstrained solution phases, Cu(II) ion can support irregular geometries that are far from the symmetric ideal. These experimental results should provide a stimulating challenge to current computational theory.[36,60,106–108]

Acknowledgment. M.B. acknowledges financial support from the SSRL Structural Molecular Biology program during a two-month stay as a visiting scientist. We thank one anonymous reviewer whose patient criticism helped improve the work described herein. This work was supported by grant NIH RR-01209 (to K.O.H.). XAS data were measured at SSRL, which is supported by the Department of Energy, Office of Basic Energy Sciences Division. The SSRL Structural Molecular Biology Program is supported by the National Institutes of Health, National Center for Research Resources, Biomedical Technology Program and by the Department of Energy, Office of Biological and Environmental Research (BER). The project described was also supported by Grant Number RR001209 from the National Center for Research Resources (NCRR), a component of the National Institutes of Health (NIH), and its contents are solely the responsibility of the authors and do not necessarily represent the official view of NCRR or NIH.

Supporting Information Available: Figures showing the speciation diagram for 0.10 M Cu^{2+} in 4 M aqueous ammonia solution, copper K-edge XAS spectra, change with axial distance, Fourier transform copper K-edge EXAFS spectra, and K-edge EXAFS spectra, tables showing comparison of the EXAFS fits for the axially elongated square pyramidal and axially elongated octahedral fit core models, comparison of the EXAFS fits for the axially symmetric elongated octahedral and axially dissymmetric core models, comparison of the EXAFS fits for the axially symmetric elongated octahedral and axially dissymmetric models, each with six second-shell N,O scatterers, MXAN fit using primitive structural models plus a second shell of four water molecules, and a Mol-format file for the final MXAN model of $\{[Cu(NH_3)_5(H_2O)]^{2+}\cdot 6H_2O$. This material is available free of charge via the Internet at http://pubs.acs.org.

IC7021243

(92) Shehu, A.; Clementi, C.; Kavraki, L. E. *Prot. Struct. Funct. Bioinform.* **2006**, *65*, 164–179.
(93) Sagle, L. B.; Zimmermann, J.; Matsuda, S.; Dawson, P. E.; Romesberg, F. E. *J. Am. Chem. Soc.* **2006**, *128*, 7909–7915.
(94) Shehu, A.; Kavraki, L. E.; Clementi, C. *Biophys. J.* **2007**, *92*, 1503–1511.
(95) Bertini, I.; Bryant, D. A.; Cuirli, S.; Dikyi, A.; Fernández, C. O.; Luchinat, C.; Safrov, N.; Vila, A. J.; Zhao, J. *J. Biol. Chem.* **2001**, *276*.
(96) Korzhnev, D. M.; Karlsson, B. G.; Orekhov, V. Y.; Billeter, M. *Protein Sci.* **2003**, *12*, 56–65.
(97) Solomon, E. I.; Szilagyi, R. K.; DeBeer George, S.; Basumallick, L. *Chem. Rev.* **2004**, *104*, 419–458.
(98) Szilagyi, R. K.; Solomon, E. I. *Curr. Opin. Chem. Biol.* **2002**, *6*, 250–258.
(99) Pasquarello, A.; Petri, I.; Salmon, P. S.; Parisel, O.; Car, R.; Tóth, É.; Powell, D. H.; Fischer, H. E.; Helm, L.; Merbach, A. E. *Science* **2001**, *291*, 856–859.
(100) Thompson, J. S.; Marks, T. J.; Ibers, J. A. *Proc. Natl. Acad. Sci. U.S.A.* **1977**, *74*, 3114–3118.
(101) Guss, J. M.; Harrowell, P. R.; Murata, M.; Norris, V. A.; Freeman, H. C. *J. Mol. Biol.* **1986**, *192*, 361–387.
(102) Brader, M. L.; Dunn, M. F. *J. Am. Chem. Soc.* **1990**, *112*, 4585–4587.
(103) Guss, J. M.; Bartunik, H. D.; Freeman, H. C. *Acta Crystallogr. B* **1992**, *48*, 790–811.
(104) Frank, P.; Licht, A.; Tullius, T. D.; Hodgson, K. O.; Pecht, I. *J. Biol. Chem.* **1985**, *260*, 5518–5525.
(105) Ryde, U.; Olsson, M. H. M.; Roos, B. O.; Borin, A. C. *Theor. Chem. Acc.* **2001**, *105*, 452–462.
(106) Schwenk, C. F.; Rode, B. M. *ChemPhysChem* **2003**, *4*, 931–943.
(107) Blumberger, J.; Bernasconi, L.; Tavernelli, I.; Vuilleumier, R.; Sprik, M. *J. Am. Chem. Soc.* **2004**, *126*, 3928–3938.
(108) Schwenk, C. F.; Rode, B. M. *ChemPhysChem* **2004**, *5*, 342–348.